Extreme Mechanics Letters 64 (2023) 102078

Contents lists available at ScienceDirect

Extreme Mechanics Letters

journal homepage: www.elsevier.com/locate/eml

Bayesian optimisation of hexagonal honeycomb metamaterial

I. Kuszczak [a], F.I. Azam [a], M.A. Bessa [b], P.J. Tan [a], F. Bosi [a,c,*]

[a] Department of Mechanical Engineering, University College London, UK
[b] School of Engineering, Brown University, USA
[c] Department of Innovative Technologies, University of Applied Sciences and Arts of Southern Switzerland, Switzerland

ARTICLE INFO

Article history:
Received 18 June 2023
Received in revised form 20 July 2023
Accepted 2 September 2023
Available online 9 September 2023

Keywords:
Architected materials
Lattices
Optimisation
Auxetic materials
Machine learning mechanics

ABSTRACT

Periodic mechanical metamaterials, such as hexagonal honeycombs, have traditionally been designed with uniform cell walls to simplify manufacturing and modelling. However, recent research has suggested that varying strut thickness within the lattice could improve its mechanical properties. To fully explore this design space, we developed a computational framework that leverages Bayesian optimisation to identify configurations with increased uniaxial effective elastic stiffness and plastic or buckling strength. The best topologies found, representative of relative densities with distinct failure modes, were additively manufactured and tested, resulting in a 54% increase in stiffness without compromising the buckling strength for slender architectures, and a 63% increase in elastic modulus and a 88% increase in plastic strength for higher volume fractions. Our results demonstrate the potential of Bayesian optimisation and solid material redistribution to enhance the performance of mechanical metamaterials.

1. Introduction

Architected materials represent a class of metamaterials whose unique mechanical properties, unattainable in conventional solids, are introduced through a rational design of their geometry and combination of different constituent materials [1–4]. Examples of material properties and functionalities created within mechanical metamaterial include negative stiffness [5] and refraction [6], superelasticity [7], extreme auxeticity [8,9], tunable band gaps [10], remarkable stiffness and strength-to-weight ratios [11,12], reconfigurability and multi-physics characteristics [13], to name a few. The significant research advances obtained over the last two decades have been fostered by the development of additive manufacturing (AM) techniques, which enable the micro- and nano-fabrication of complex structured materials with precise control over their geometry and various constituent materials [14–16]. Although AM offers the possibility of fabricating a plethora of topologies, most mechanical metamaterials designed and realised to date are regular periodic truss-, beam-, plate-, and shell-based configurations characterised by cell walls with uniform thickness and cross-section [17,18], mainly for ease of analytical modelling and traditional fabrication. Such regular solid material distribution often results in suboptimal mechanical properties because of the inhomogeneous stress and strain distributions present along the cell walls for most of the lattice topologies and loading conditions. Bending-dominated lattices – which deform primarily by bending their cell walls – can benefit the most from shape optimisation of their strut to redistribute material where it is most needed. Previous studies, mainly focusing on hexagonal honeycombs, have shown (through analytical, numerical and experimental techniques) that the redistribution of solid material leads to an enhancement of elastic lattice properties [19–27]. Nevertheless, those attempts assumed a predefined variable strut thickness guided by designers' experience or experimental observations, which prevent the exploration of untapped regions of the design space and therefore limit the potential gain in mechanical properties.

To overcome these limitations, topology optimisation (TO) has been employed alongside computational homogenisation techniques to seek optimal solid material distribution in unit cell of periodic lattices and improve single static and dynamic macroscopic elastic properties [28,29]. More recently, TO has been applied to enhance the design of mechanical metamaterials by simultaneously maximising stiffness and strength [30], considering non-uniform [31] or multi-material lattices via a multi-scale approach [32]. Within this framework, machine learning and deep learning are alternative techniques that can favour the creation of metamaterials for different applications. They offer a fast and efficient search for optimal configurations in large design spaces difficult to manage by conventional methods, while providing surrogate models of the properties of interest as a function of the design variables [33–38]. Bayesian optimisation (BO) is

* Corresponding author at: Department of Mechanical Engineering, University College London, UK.
E-mail address: f.bosi@ucl.ac.uk (F. Bosi).

https://doi.org/10.1016/j.eml.2023.102078

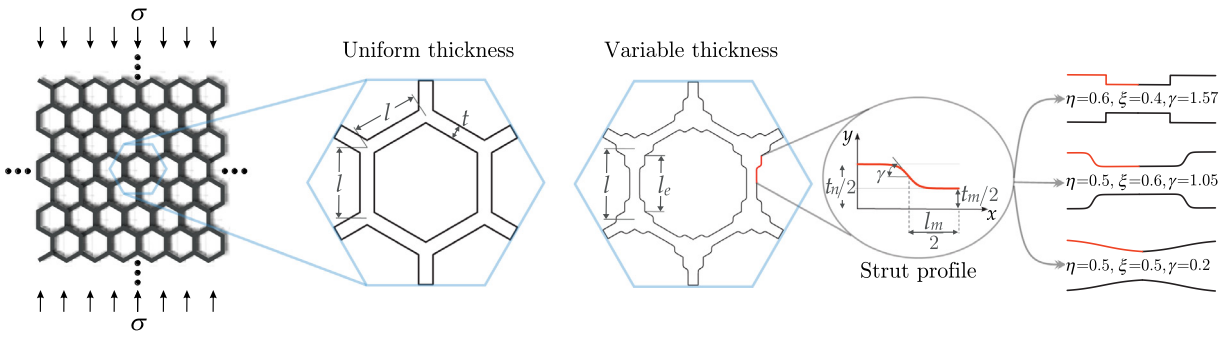

Fig. 1. Regular hexagonal lattice and unit cell with uniform and variable strut thickness. The strut profile for the unit cell with solid material redistributed is shown in red, alongside the three independent design parameters η, ξ, γ and three configurations obtainable through the chosen shape parametrisation. (For interpretation of the references to colour in this figure legend, the reader is referred to the web version of this article.)

a particularly desirable approach in the context of metamaterial optimisation because it limits the extensive pre-sampling of the design space while being able to deal with noisy objective function evaluations and quantifying uncertainty, which results useful when dealing with small-scale architectures sensitive to manufacturing imperfections and instabilities [39,40].

In this letter, we aim to demonstrate that such a data-driven approach offers a breakthrough in the optimisation of mechanical properties of architected metamaterials through solid material redistribution. In particular, we advance on the previous approaches by treating material redistribution in the cell walls as a parametric shape optimisation problem. Although the choice of parametrisation inherently constrains the design space, the approach offers notable advantages compared to the more general TO approach. Firstly, parametrisations can implicitly enforce manufacturing constraints, ensuring that the resulting material redistribution design is not only optimised but also feasible and practical to manufacture. Secondly, as demonstrated later in this study, the approach readily applies to scenarios where different topologies present different failure modes. Lastly, the BO approach provides not only the optimal solution but also computationally cheap metamodels that enable designers to evaluate the evolution of mechanical properties over the entire design space and select different configurations depending on additional considerations.

2. Model and methodology

Without loss of generality, we illustrate the conceived methodology on the parametric shape optimisation of a regular two-dimensional bending-dominated hexagonal honeycomb subjected to uniaxial compression. The material along the cell walls is redistributed to increase the elastic stiffness and strength of the uniform thickness lattice, for the same mass and relative density $\overline{\rho}$ (defined as the density ratio of lattice material to the solid material of equivalent size). Regular periodic honeycombs are characterised by struts, or cell walls, of constant length l and thickness t, as shown in Fig. 1(left). Their effective mechanical properties can be analytically found as a function of $\overline{\rho}_u (= 2t/(\sqrt{3}l) - t^2/(3l^2))$ as [17]

$$\frac{E_u}{E_s} = \frac{3}{2}\overline{\rho}_u^3, \quad \frac{\sigma_{y,u}}{\sigma_{y,s}} = \frac{1}{2}\overline{\rho}_u^2, \quad \frac{\sigma_{b,u}}{E_s} = 0.143\,\overline{\rho}_u^3 \tag{1}$$

where E, σ_y and σ_b are Young's modulus, plastic and buckling strengths, respectively. The subscripts u and s denote the properties of the lattice with uniform thickness and that of its constituent material, respectively. The scaling laws above are obtained using the first-order approximation of the relative density, neglecting the second-order term of t/l, which means the expressions are only valid for low relative densities or high strut slenderness ratios. However, those expressions are not used in this work, where the mechanical properties of uniform and non-uniform honeycombs are computed directly from the finite element analyses, as described in the following.

The non-uniform hexagonal honeycombs with variable thickness (indicated by the subscript v) are obtained by redistributing solid material from the middle of the strut (region of low bending moment) towards the end, or nodal, section (region of high bending moment). The profile of the cell wall is described through a parametrisation that guarantees several strut shapes, as shown in Fig. 1(right). Exploiting symmetry along the longitudinal axis x and middle section, the shape of a quarter of a strut with an effective length l_e and middle thickness t_m is modelled using a hyperbolic tangent function described by

$$y(x) = y_0 + \alpha \tanh\left(\frac{\tan\gamma}{\alpha}(x_0 - x)\right), \qquad x \in \left[0, \frac{l_e}{2}\right], \tag{2}$$

where $l_e \approx l - \sqrt{3}t_m/(3\eta)$, $y_0 = t_m/4(1/\eta + 1)$, $x_0 = l_e(1-\xi)/2$ and $\alpha = t_m/4(1/\eta - 1)$. The parametrisation was set up so that each parameter has a well-defined meaning: $\eta \in (0, 1]$ is the ratio of the middle section thickness t_m to the nodal section thickness t_n, $\xi \in [0, 1]$ is the ratio of the middle section length l_m to beam's effective length l_e, and $\gamma \in [0, \pi/2]$ is the angle (in radians) between the transition section at $x = x_0$ and the longitudinal x-axis.

The analytical expression of the strut profile enables the calculation of relative density $\overline{\rho}_v$ of the non-uniform honeycomb with variable thickness, which depends on l, t_m, η, ξ and γ, as reported in the Supplementary Material (SM). Since the objective of the work is to improve the mechanical properties by redistributing material while keeping constant the total mass (volume) and strut length l, a relative density equivalency has to be established between the uniform and non-uniform honeycombs, $\overline{\rho}_u = \overline{\rho}_v (= \overline{\rho})$. Therefore, for each parametrisation considered, t_m can be expressed as a function of t, and the three-dimensional design space of the non-uniform honeycomb is constituted by the parameters η, ξ and γ.

The workflow of the data-driven shape optimisation of hexagonal honeycomb is summarised in Fig. 2 and described in more detail in the SM. Once the relative density $\overline{\rho}$ and the strut length l are set, the unit cell of the variable thickness honeycomb is generated through the parametrisation described above, with t_m obtained from the relative density equivalency. Different designs are originated by sampling the bounded three-dimensional design space using a quasi-random low-discrepancy Sobol sequence, to facilitate the subsequent machine learning step [36].

Each design is then imported into the Finite Element (FE) software to predict the compressive behaviour and build a response database, to be used in the learning and optimisation processes,

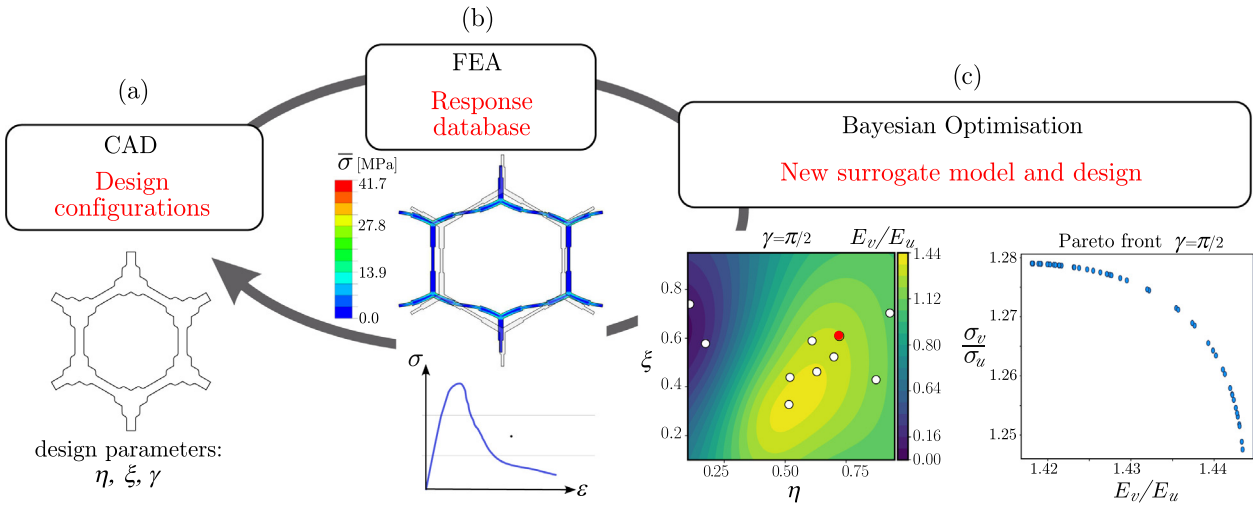

Fig. 2. Illustration of the computational framework for the parametric shape optimisation of periodic metamaterials applied to hexagonal lattices with three design parameters.

see Fig. 2(b). Nonlinear finite element analyses are carried out on unit cells with translational symmetry, where periodic boundary conditions are imposed on each side pair to obtain the bulk properties of the infinite-sized lattices while reducing the computational time [41–43] (details in Sect. 1.3, SM). Considering the two-dimensional geometry and its loading condition, plane stress elements were used to discretise the unit cells. A remote uniaxial compressive strain is imposed along the vertical direction because both uniform and non-uniform honeycombs are isotropic in the linear elastic regime. However, it should be noted that nonlinear geometric effects and plasticity cause on both geometries direction-dependent peak stresses and softening responses. Vertical (with respect to the unit cell orientation of Fig. 1) compression produces a stronger response until the peak stress and a more pronounced softening phase compared to that observable during uniaxial horizontal compression. The constituent material model is elastic perfectly-plastic, characterised by the average experimentally determined Young's modulus $E_s = 893.15$ MPa and yield stress $\sigma_{y,s} = 38.99$ MPa (details in Sect. 2, SM). It should be noted that, although the material assumed for the FE simulations corresponds to that of the experiments, the lattice properties of interest are normalised by those of the uniform honeycomb. Hence, they result independent on the chosen constituent material properties and only dependent on the geometry. For each design and numerical experiment, the critical buckling stress of the honeycomb, $\sigma_{b,v}$, and the lattice effective stress–strain response, σ vs. ε, are obtained from linear perturbation and quasi-static steps of the FE analysis, respectively. From the latter, the effective elastic stiffness, or Young's modulus, of the lattice E_v is computed along with its plastic collapse strength $\sigma_{y,v}$, defined as the peak stress at which plastic hinges form, followed by softening. The unit cell mode of failure, either elastic buckling (for $\overline{\rho} < \overline{\rho}_c$, where $\overline{\rho}_c$ is the shape-dependent critical relative density that distinguishes buckling from plastic collapse) or yielding (for $\overline{\rho} > \overline{\rho}_c$), is defined by the minimum failure strength, $\sigma_v = \min[\sigma_{b,v}, \sigma_{y,v}]$.

Subsequently, the lattice properties of interest, normalised by those of the uniform honeycomb obtained via FE, E_v/E_u, $\sigma_{b,v}/\sigma_{b,u}$ and $\sigma_{y,v}/\sigma_{y,u}$, are maximised with Bayesian optimisation. After each evaluation, a probabilistic surrogate model, specifically a Gaussian process, is fit to the known data and used to predict how the mechanical properties of interest evolve based on the design parameters. This iterative process allows for a more efficient and accurate understanding of the relationship between the design parameters and lattice properties, ultimately aiding in the optimisation of the material's mechanical behaviour. The illustrative example of Fig. 2(c) shows a projection of the design space (ξ vs. η, for $\gamma = \pi/2$), where the contour plot highlights the changes of normalised elastic stiffness E_v/E_u. Some training data points can be observed, alongside the region where the solid material redistribution is effectively enhancing the stiffness of the uniform honeycomb, $E_v/E_u > 1$. The Multi-Objective Bayesian Optimisation (MOBO) step aims at finding Pareto optimal solutions in the presence of competing objectives, while minimising the number of performed evaluations. The search for the optimal configuration is guided by the Expected Hypervolume Improvement acquisition function [44], in a trade-off between exploration of regions of the design space with high uncertainty and exploitation of the areas with potentially high objective functions' values. Hence, a new parametrisation with the highest probability of achieving a higher hypervolume is (i) selected, (ii) its CAD created, (iii) its response predicted by FE, and (iv) new probabilistic models of the quantities of interests (E_v/E_u, $\sigma_{b,v}/\sigma_{b,u}$ and $\sigma_{y,v}/\sigma_{y,u}$) updated after each evaluation, in an iterative approach that converges towards the true Pareto front. The final Pareto front is used in conjunction with the Technique for Order of Preference by Similarity to Ideal Solution (TOPSIS) to select the best design [45].

3. Results and discussion

The presented data-driven framework is applied to the shape optimisation through material redistribution of hexagonal honeycombs of relative densities $\overline{\rho} = 0.10$ and $\overline{\rho} = 0.23$, representative of configurations that undergo buckling and plastic collapse, respectively. The trials evaluated in the optimisation processes are reported in Fig. 3(left), showing a good sampling of the three-dimensional design space, especially towards the combination of parameters that guarantee enhanced mechanical properties. The consecutive trials of the MOBO are shown in the objective space of the problem σ_v/σ_u vs. E_v/E_u, Fig. 3(centre), proving that the procedure quickly converges and identifies promising designs that trade-off high stiffness and strength ratios. Considering the presence of competing mechanical properties, Fig. 3(right) shows a combination of Pareto optimal (non-dominated) configurations obtained from actual trials as well as predictions from the posterior surrogate model. Although the shape of the Pareto front is similar for both relative densities, the values of the best objective properties achievable, especially strength, differ considerably.

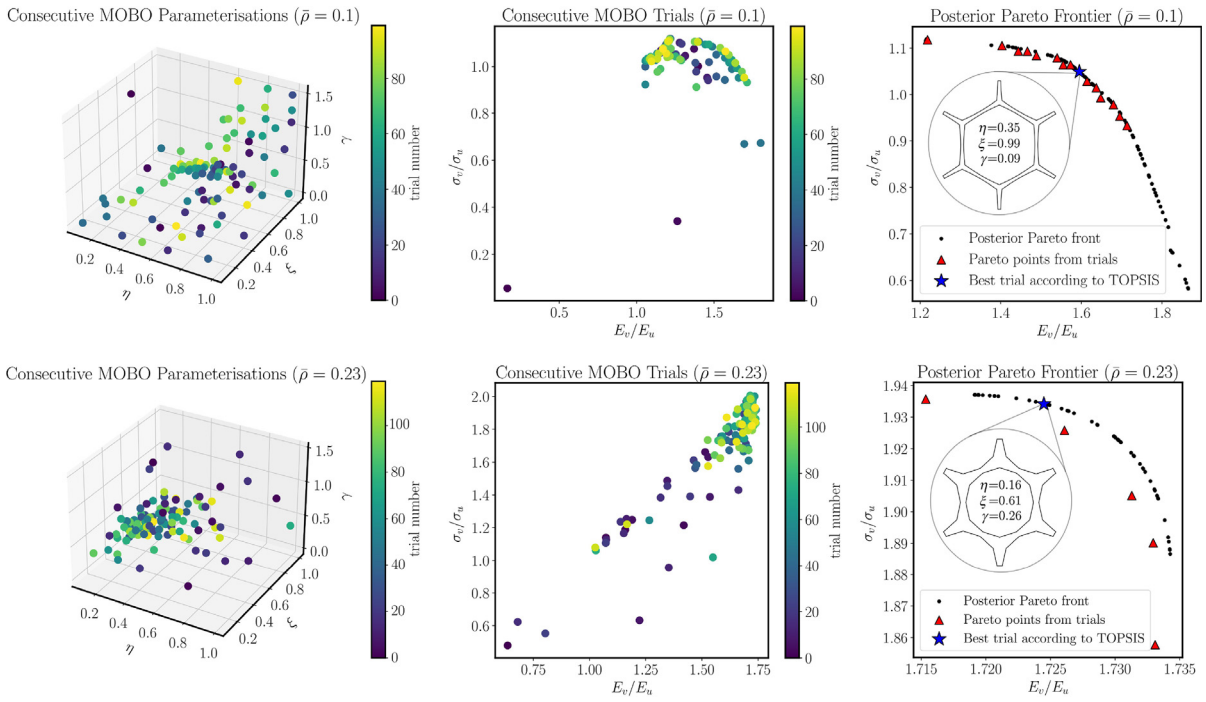

Fig. 3. Results obtained from the Bayesian optimisation process for the parametric shape optimisation of hexagonal lattices with relative densities $\overline{\rho} = 0.10$ (top) and $\overline{\rho} = 0.23$ (bottom). For each relative density, the training points are shown in the design space (left) and in the plane of normalised quantities of interest σ_v/σ_u vs. E_v/E_u (centre), where values higher than one testify an improvement of mechanical properties with respect to uniform thickness honeycomb. The posterior front (right) highlights the Pareto optimal solutions and the selected configuration.

This behaviour can be explained by the different failure modes of the two configurations. When $\overline{\rho} = 0.10$, the loss of load-carrying capacity is caused by elastic buckling and the limited strength improvement compared to the uniform honeycomb is attributed to the ineffectiveness of the assumed material redistribution in axial instability phenomena, for which a reduction of the cross-section (and second moment of area) in the central region of the cell wall can lead to a significant decrease of the buckling stress. Nevertheless, Bayesian optimisation was able to pinpoint the best honeycomb shape with $\sigma_v/\sigma_u = 1.05$ and $E_v/E_u = 1.59$ within 100 iterations. Improved buckling stress could be obtained by considering a hierarchical design that reduces the effective struts length, thus increasing their buckling load [28]. For $\overline{\rho} = 0.23$, the lattice fails primarily due to plastic collapse. In this scenario, a solid redistribution that follows the bending moment evolution along the strut's longitudinal axis, with more material at the nodal section and less at the centre, can simultaneously increase the yield strength and elastic stiffness up to $\sigma_v/\sigma_u = 1.93$ and $E_v/E_u = 1.72$.

It should be noted that both best strut configurations were found to assume an almost tapered profile, as was expected from the linear variation of the bending moment in the inclined strut predicted by beam theory [19]. Such best configurations are named as 'optimised' in the context of Bayesian optimisation, where the TOPSIS best (optimal) shape is found by ranking the points given the assumption on the design space and the information on the surrogate model. However, it is acknowledged that the assumed parametric shape equation defining the evolution of strut thickness, which maintains an hexagonal-like unit cell topology, reduce the design space. If this hypothesis is relaxed, other topologies with enhanced mechanical properties could be obtained, for example through topology optimisation [28,30,32]. However, such approach would not yield a surrogate model of the design objectives nor provide uncertain quantification.

Based on the computational results, we additively manufactured the optimised configurations to validate the data-driven approach. Uniform and shape-optimised honeycombs with $\overline{\rho} = 0.10$ and $\overline{\rho} = 0.23$ were fabricated with a photo-curable resin through stereolithography technique (full details of the experimental method in the SM). The finite lattices consisted of 10×9 cells (width $\times$ height) to achieve mechanical properties within 90% of the bulk value from unit cell analysis [46]. The minimum strut thickness was set to 0.5 mm and 0.75 mm for the $\overline{\rho} = 0.10$ and $\overline{\rho} = 0.23$ lattices, respectively, while the depth of the specimens was $D = 20$ mm to avoid out-of-plane instabilities. Compression experiments were performed under quasi-static conditions by imposing a vertical displacement to the lattice and measuring the resulting force, from which the effective engineering stress (normalised by the failure strength of the uniform honeycomb, $\sigma_u = \min[\sigma_{b,u}, \sigma_{y,u}]$) vs. strain responses were calculated. They are reported (solid curves) and compared to the FE predictions (dashed curves) of the unit cell and of the finite lattice in Fig. 4(a) and (b) for the two relative densities considered. The FE results for the finite lattices were obtained by using an adaptive mesh constituted of plane stress elements that discretise the CAD geometry of the manufactured samples, in a trade-off between accuracy and computational time. The boundary and loading conditions reproduced those of the experiments, with the finite lattices compressed through rigid and frictional platens, while self-contact properties were defined on all surfaces of the lattice to capture the response at high remote strains (details in Sect. 1.3, SM).

Focusing only on the region until the first peak stress, where the mechanical properties of interest are optimised, it can be observed that the elastic stiffness and strength of both best configurations are well above those of the uniform honeycombs, for the same relative density. This proves the effectiveness of the material redistribution strategy and the Bayesian shape optimisation. In particular, for $\overline{\rho} = 0.10$, the measured increase in stiffness with respect to the uniform lattice is 54%, while the buckling strength is reduced by 5%. The marginally lower improvement of mechanical properties achieved experimentally,

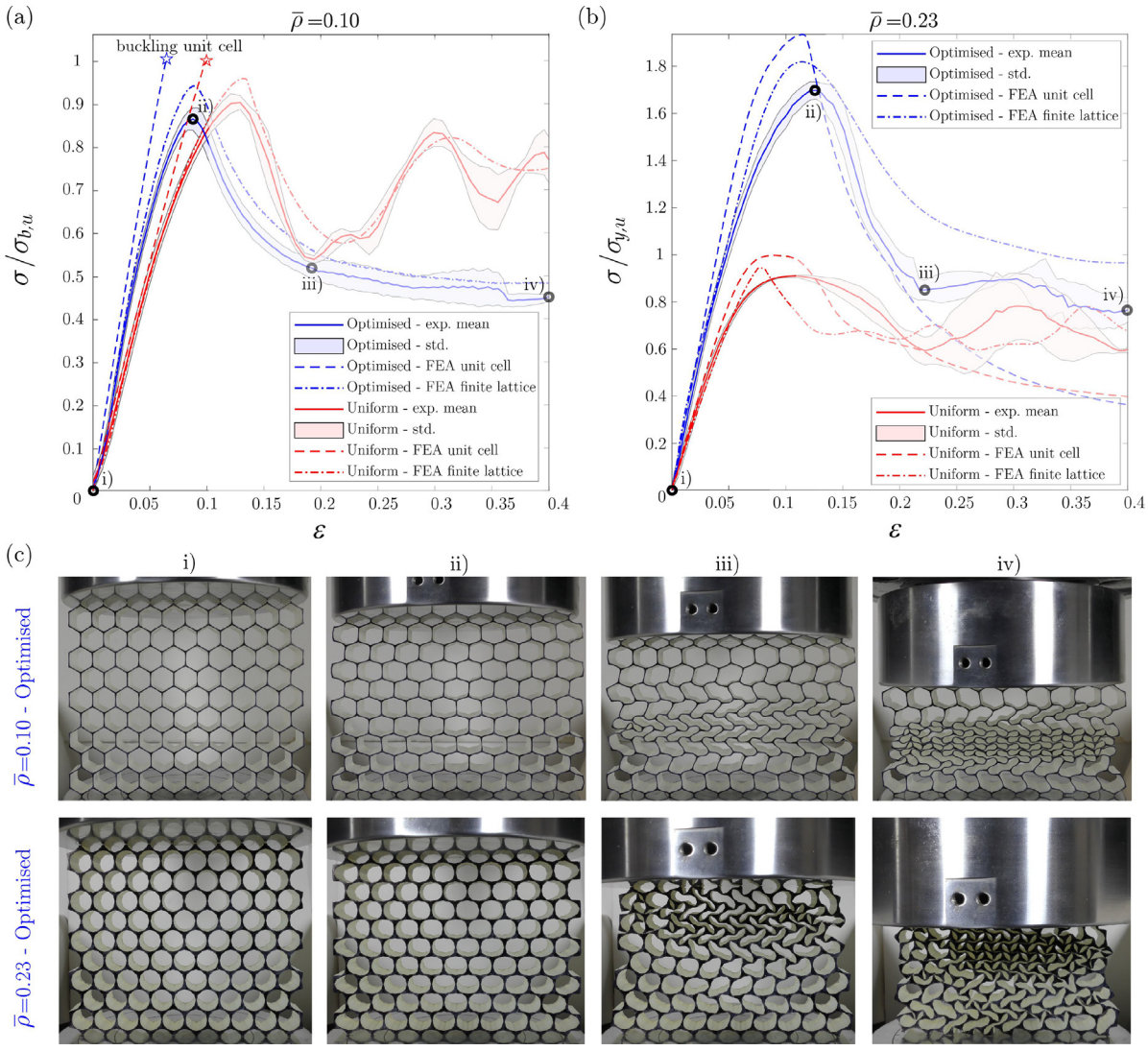

Fig. 4. Compressive stress–strain response of hexagonal honeycombs with uniform (red) and optimised (blue) strut thickness profile for $\overline{\rho} = 0.10$ (a) and $\overline{\rho} = 0.23$ (b). Experimental measurements (average and standard deviation, solid curves) are reported together with FE results for unit cell (dashed curves) and finite lattice (dot-dashed curves). The region after the first peak stress is shown with higher transparency because was not part of the mechanical properties optimisation, limited to stiffness and buckling or plastic strength. (c) Images from the compression experiments on optimised design at increasing remote strain, taken from the experimental mean (blue solid) curves of plots (a) and (b), as highlighted by points (i) to (iv). Images (i) represent the virgin samples, (ii) the configurations at the peak stress, while (iii) and (iv) show an auxetic response of the non-uniform lattices beyond the peak stress. (For interpretation of the references to colour in this figure legend, the reader is referred to the web version of this article.)

compared with that computationally obtained via unit cell analysis, is attributed to the slightly lower relative density (ca. 3%) of the optimised lattices. If experiments are carried out on uniform and non-uniform lattices with the same relative density, the gain achievable would be higher, as shown in Table II, SM. For $\overline{\rho} = 0.23$, the experimental gains in Young's modulus and plastic strength are 63% and 88%, respectively (see also Table II, SM). When the measured responses are compared with FE predictions, it can be observed that there is good agreement with the results from the finite lattices. They resulted ≈10% lower than the infinite lattice (unit cell analysis) because the edge effects of the finite samples reduce the uniaxial compressive properties [46]. The minor discrepancies between the finite-sized FE results and experiments, especially in the non-uniform geometries, are attributed to their higher sensitivity to manufacturing imperfections. We note that imperfection sensitivity can also be included in the data-driven optimisation process, as demonstrated previously [36], if the nominal shape of the metamaterial is perturbed by an amplitude estimated from the manufacturing process. However, since significant discrepancies have not been observed, this avenue was not pursued.

Although the post-failure regime was not part of the optimisation procedure, it is worth noting that the stress–strain plots of the uniform and non-uniform honeycombs, as well as finite or infinite lattices, show different softening responses, as discussed in the SM. Moreover, from Fig. 4(c) and SM Fig. 6, it can be observed that the material redistribution not only enhances the mechanical properties, but has also reduced the effective Poisson's ratio of the uniform honeycomb. A pronounced strain-dependent auxetic response develops beyond the linear elastic regime, where the minimum Poisson's ratio of the non-uniform lattice reaches $\nu_{v,\min,0.10} \approx -0.13$ and $\nu_{v,\min,0.23} \approx -0.58$. By contrast, the measured Poisson's ratio of the uniform honeycomb always remains positive, ranging from $\nu_{u,\max} \approx 0.97$ in the linear elastic phase to $\nu_{u,\min} \approx 0.22$ at the maximum imposed strain.

4. Conclusion

In conclusion, we demonstrated significant enhancements of mechanical metamaterial properties through solid material redistribution. Furthermore, we have shown that data-driven multi-objective Bayesian optimisation is a valuable tool for exploring complex design spaces to achieve lighter, stiffer, and stronger topologies. Although we utilised this framework on relatively simple hexagonal unit cell topologies, where mechanics knowledge and intuition could have been sufficient to propose a tapered cell wall profile, it has even greater potential for problems where the underlying objective function is not well-understood or where intuition may not be enough. The ability of Bayesian optimisation to converge to optimal solutions with a limited evaluation budget is a clear indication of its efficacy. Its potential in solving more complex optimisation problems in multi-physics and other domains is therefore highly anticipated.

Declaration of competing interest

The authors declare that they have no known competing financial interests or personal relationships that could have appeared to influence the work reported in this paper.

Data availability

Data will be made available on request.

Acknowledgement

The authors acknowledge support from the EU H2020-MSCA-ITN-2020-LIGHTEN-956547.

Appendix A. Supplementary data

Supplementary material related to this article can be found online at https://doi.org/10.1016/j.eml.2023.102078.

References

[1] N.A. Fleck, V.S. Deshpande, M.F. Ashby, Micro-architectured materials: past, present and future, Proc. R. Soc. A 466 (2121) (2010) 2495–2516, http://dx.doi.org/10.1098/rspa.2010.0215.
[2] J.U. Surjadi, L. Gao, H. Du, X. Li, X. Xiong, N.X. Fang, Y. Lu, Mechanical metamaterials and their engineering applications, Adv. Eng. Mater. 21 (3) (2019) 1800864, http://dx.doi.org/10.1002/adem.201800864.
[3] J. Bauer, L.R. Meza, T.A. Schaedler, R. Schwaiger, X. Zheng, L. Valdevit, Nanolattices: An emerging class of mechanical metamaterials, Adv. Mater. 29 (40) (2017) 1701850, http://dx.doi.org/10.1002/adma.201701850.
[4] K. Bertoldi, V. Vitelli, J. Christensen, M. Schwaiger, Flexible mechanical metamaterials, Nat. Rev. Mater. 2 (11) (2017) 17066, http://dx.doi.org/10.1038/natrevmats.2017.66.
[5] B.M. Goldsberry, M.R. Haberman, Negative stiffness honeycombs as tunable elastic metamaterials, J. Appl. Phys. 123 (9) (2018) 091711, http://dx.doi.org/10.1063/1.5011400.
[6] X. Zhang, Z. Liu, Negative refraction of acoustic waves in two-dimensional phononic crystals, Appl. Phys. Lett. 85 (2) (2004) 341–343, http://dx.doi.org/10.1063/1.1772854.
[7] Q. Zhang, X. Xu, D. Lin, W. Chen, G. Xiong, Y. Yu, T.S. Fisher, H. Li, Hyperbolically patterned 3D graphene metamaterial with negative Poisson's ratio and superelasticity, Adv. Mater. 28 (11) (2016) 2229–2237, http://dx.doi.org/10.1002/adma.201505409.
[8] D. Misseroni, P.P. Pratapa, K. Liu, G.H. Paulino, Experimental realization of tunable Poisson's ratio in deployable origami metamaterials, Extreme Mech. Lett. 53 (2022) 101685, http://dx.doi.org/10.1016/j.eml.2022.101685.
[9] A. Desmoulins, A.J. Zelhofer, D.M. Kochmann, Auxeticity in truss networks and the role of bending versus stretching deformation, Smart Mater. Struct. 25 (5) (2016) 054003, http://dx.doi.org/10.1088/0964-1726/25/5/054003.
[10] M. Gei, Z. Chen, F. Bosi, L. Morini, Phononic canonical quasicrystalline waveguides, Appl. Phys. Lett. 116 (24) (2020) 241903, http://dx.doi.org/10.1063/5.0013528.
[11] A. Kudo, F. Bosi, Nanographitic coating enables hydrophobicity in lightweight and strong microarchitected carbon, Commun. Mater. 1 (2020) http://dx.doi.org/10.1038/s43246-020-00073-3.
[12] A. Kudo, D. Misseroni, Y. Wei, F. Bosi, Compressive response of non-slender octet carbon microlattices, Front. Mater. 6 (2019) 169, http://dx.doi.org/10.3389/fmats.2019.00169.
[13] X. Xia, A. Afshar, H. Yang, C.M. Portela, D.M. Kochmann, C.V. Di Leo, J.R. Greer, Electrochemically reconfigurable architected materials, Nature 573 (7773) (2019) 205–213, http://dx.doi.org/10.1038/s41586-019-1538-z.
[14] X. Zhang, A. Vyatskikh, H. Gao, J.R. Greer, X. Li, Lightweight, flaw-tolerant, and ultrastrong nanoarchitected carbon, Proc. Natl. Acad. Sci. 116 (14) (2019) 6665–6672, http://dx.doi.org/10.1073/pnas.1817309116.
[15] L.R. Meza, S. Das, J.R. Greer, Strong, lightweight, and recoverable three-dimensional ceramic nanolattices, Science 345 (6202) (2014) 1322–1326, http://dx.doi.org/10.1126/science.1255908.
[16] X. Zheng, W. Smith, J. Jackson, B. Moran, H. Cui, D. Chen, J. Ye, N. Fang, N. Rodriguez, T. Weisgraber, et al., Multiscale metallic metamaterials, Nat. Mater. 15 (10) (2016) 1100–1106, http://dx.doi.org/10.1038/nmat4694.
[17] L. Gibson, M. Ashby, Cellular Solids: Structure and Properties, in: Cambridge Solid State Science Series, Cambridge University Press, 1999, http://dx.doi.org/10.1017/CBO9781139878326.
[18] S. Malek, L. Gibson, Effective elastic properties of periodic hexagonal honeycombs, Mech. Mater. 91 (2015) 226–240, http://dx.doi.org/10.1016/j.mechmat.2015.07.008.
[19] C. Chen, T. Lu, N. Fleck, Effect of imperfections on the yielding of two-dimensional foams, J. Mech. Phys. Solids 47 (11) (1999) 2235–2272, http://dx.doi.org/10.1016/S0022-5096(99)00030-7.
[20] K. Li, X.-L. Gao, G. Subhash, Effects of cell shape and cell wall thickness variations on the elastic properties of two-dimensional cellular solids, Int. J. Solids Struct. 42 (5) (2005) 1777–1795, http://dx.doi.org/10.1016/j.ijsolstr.2004.08.005.
[21] L. Zhang, B. Liu, Y. Gu, X.H. Xu, Modelling and characterization of mechanical properties of optimized honeycomb structure, Int. J. Mech. Mater. Des. 16 (2020) 155–166, http://dx.doi.org/10.1007/s10999-019-09462-0.
[22] C.-H. Chuang, J.-S. Huang, Effects of solid distribution on the elastic buckling of honeycombs, Int. J. Mech. Sci. 44 (7) (2002) 1429–1443, http://dx.doi.org/10.1016/S0020-7403(02)00039-5.
[23] M.-Y. Yang, J.-S. Huang, Elastic buckling of regular hexagonal honeycombs with plateau borders under biaxial compression, Compos. Struct. 71 (2) (2005) 229–237, http://dx.doi.org/10.1016/j.compstruct.2004.10.014.
[24] L. Zhang, S. Feih, S. Daynes, Y. Wang, M.Y. Wang, J. Wei, W.F. Lu, Buckling optimization of Kagome lattice cores with free-form trusses, Mater. Des. 145 (2018) 144–155, http://dx.doi.org/10.1016/j.matdes.2018.02.026.
[25] A. Simone, L. Gibson, Effects of solid distribution on the stiffness and strength of metallic foams, Acta Mater. 46 (6) (1998) 2139–2150, http://dx.doi.org/10.1016/S1359-6454(97)00421-7.
[26] A. Zargarian, M. Esfahanian, J. Kadkhodapour, S. Ziaei-Rad, Effect of solid distribution on elastic properties of open-cell cellular solids using numerical and experimental methods, J. Mech. Behav. Biomed. Mater. 37 (2014) 264–273, http://dx.doi.org/10.1016/j.jmbbm.2014.05.018.
[27] T.-C. Lin, M.-Y. Yang, J.-S. Huang, Effects of solid distribution on the out-of-plane elastic properties of hexagonal honeycombs, Compos. Struct. 100 (2013) 436–442, http://dx.doi.org/10.1016/j.compstruct.2013.01.007.
[28] C.R. Thomsen, F. Wang, O. Sigmund, Buckling strength topology optimization of 2D periodic materials based on linearized bifurcation analysis, Comput. Methods Appl. Mech. Engrg. 339 (2018) 115–136, http://dx.doi.org/10.1016/j.cma.2018.04.031.
[29] X. Zhang, J. Xing, P. Liu, Y. Luo, Z. Kang, Realization of full and directional band gap design by non-gradient topology optimization in acoustic metamaterials, Extreme Mech. Lett. 42 (2021) 101126, http://dx.doi.org/10.1016/j.eml.2020.101126.
[30] F. Wang, O. Sigmund, Architecting materials for extremal stiffness, yield, and buckling strength, Program. Mater. 1 (2023) e6, http://dx.doi.org/10.1017/pma.2023.5.
[31] Y. Han, W.F. Lu, A novel design method for nonuniform lattice structures based on topology optimization, J. Mech. Des. 140 (9) (2018) 091403, http://dx.doi.org/10.1115/1.4040546.
[32] M. Montemurro, T. Roiné, J. Pailhès, Multi-scale design of multi-material lattice structures through a CAD-compatible topology optimisation algorithm, Eng. Struct. 273 (2022) 115009, http://dx.doi.org/10.1016/j.engstruct.2022.115009.
[33] A. Namvar, A. Vosoughi, Design optimization of moderately thick hexagonal honeycomb sandwich plate with modified multi-objective particle swarm optimization by genetic algorithm (MOPSOGA), Compos. Struct. 252 (2020) 112626, http://dx.doi.org/10.1016/j.compstruct.2020.112626.
[34] L. Wang, H.-T. Liu, Parameter optimization of bidirectional re-entrant auxetic honeycomb metamaterial based on genetic algorithm, Compos. Struct. 267 (2021) 113915, http://dx.doi.org/10.1016/j.compstruct.2021.113915.

[35] F. Liu, X. Jiang, X. Wang, L. Wang, Machine learning-based design and optimization of curved beams for multistable structures and metamaterials, Extreme Mech. Lett. 41 (2020) 101002, http://dx.doi.org/10.1016/j.eml.2020.101002.
[36] M. Bessa, S. Pellegrino, Design of ultra-thin shell structures in the stochastic post-buckling range using Bayesian machine learning and optimization, Int. J. Solids Struct. 139–140 (2018) 174–188, http://dx.doi.org/10.1016/j.ijsolstr.2018.01.035.
[37] Z. Vangelatos, H.M. Sheikh, P.S. Marcus, C.P. Grigoropoulos, V.Z. Lopez, G. Flamourakis, M. Farsari, Strength through defects: A novel Bayesian approach for the optimization of architected materials, Sci. Adv. 7 (41) (2021) eabk2218, http://dx.doi.org/10.1126/sciadv.abk2218.
[38] K. Guo, M.J. Buehler, A semi-supervised approach to architected materials design using graph neural networks, Extreme Mech. Lett. 41 (2020) 101029, http://dx.doi.org/10.1016/j.eml.2020.101029.
[39] M.A. Bessa, P. Glowacki, M. Houlder, Bayesian machine learning in metamaterial design: Fragile becomes supercompressible, Adv. Mater. 31 (48) (2019) 1904845, http://dx.doi.org/10.1002/adma.201904845.
[40] D. Pasini, J.K. Guest, Imperfect architected materials: Mechanics and topology optimization, MRS Bull. 44 (10) (2019) 766–772, http://dx.doi.org/10.1557/mrs.2019.231.
[41] S. Li, Boundary conditions for unit cells from periodic microstructures and their implications, Compos. Sci. Technol. 68 (9) (2008) 1962–1974, http://dx.doi.org/10.1016/j.compscitech.2007.03.035.
[42] S. Li, On the unit cell for micromechanical analysis of fibre-reinforced composites, Proc. R. Soc. Lond. Ser. A Math. Phys. Eng. Sci. 455 (1983) (1999) 815–838, http://dx.doi.org/10.1098/rspa.1999.0336.
[43] S. Li, General unit cells for micromechanical analyses of unidirectional composites, Composites A 32 (6) (2001) 815–826, http://dx.doi.org/10.1016/S1359-835X(00)00182-2.
[44] S. Daulton, M. Balandat, E. Bakshy, Differentiable expected hypervolume improvement for parallel multi-objective Bayesian optimization, Adv. Neural Inf. Process. Syst. 33 (2020) 9851–9864, http://dx.doi.org/10.48550/arXiv.2006.05078.
[45] M. Méndez, M. Frutos, F. Miguel, R. Aguasca-Colomo, TOPSIS decision on approximate Pareto fronts by using evolutionary algorithms: Application to an engineering design problem, Mathematics 8 (11) (2020) 2072, http://dx.doi.org/10.3390/math8112072.
[46] P. Onck, E. Andrews, L. Gibson, Size effects in ductile cellular solids. Part I: modeling, Int. J. Mech. Sci. 43 (3) (2001) 681–699, http://dx.doi.org/10.1016/S0020-7403(00)00042-4.